Molecular Imaging

Intraperitoneal Injection Improves the Uptake of Nanoparticle-Labeled High-Density Lipoprotein to Atherosclerotic Plaques Compared With Intravenous Injection

A Multimodal Imaging Study in ApoE Knockout Mice

Caroline Jung, MD; Michael G. Kaul, MS; Oliver T. Bruns, PhD; Tanja Dučić, PhD; Barbara Freund, PhD; Markus Heine, PhD; Rudolph Reimer, PhD; Alke Meents, PhD; Sunhild C. Salmen, MS; Horst Weller, PhD; Peter Nielsen, MD; Gerhard Adam, MD; Jörg Heeren, PhD; Harald Ittrich, MD

Background—The aim of this study was to assess whether high-density lipoprotein (HDL) labeled with superparamagnetic iron oxide nanoparticles (SPIOs) and quantum dots was able to detect atherosclerotic lesions in mice after intravenous and intraperitoneal injection by multimodal imaging.

Methods and Results—Nanoparticle-labeled HDLs (NP-HDLs) were characterized in vitro by dynamic light scattering and size exclusion chromatography with subsequent cholesterol and fluorescence measurements. For biodistribution and blood clearance studies, NP-HDL_{SPIOs} radiolabeled with ⁵⁹Fe (NP-HDL_{59Fe-SPIOs}) were injected intravenously or intraperitoneally into ApoE knockout mice (n=6), and radioactivity was measured using a gamma counter. NP-HDL accumulation within atherosclerotic plaques in vivo and ex vivo was estimated by MRI at 7 Tesla, ex vivo confocal fluorescence microscopy, x-ray fluorescence microscopy, and histological analysis (n=3). Statistical analyses were performed using a 2-tailed Student t-test. In vitro characterization of NP-HDL confirmed properties similar to endogenous HDL. Blood concentration time curves showed a biexponential decrease for the intravenous injection, whereas a slow increase followed by a steady state was noted for intraperitoneal injection. Radioactivity measurements showed predominant accumulation in the liver and spleen after both application approaches. NP-HDL_{59Fe-SPIOs} uptake into atherosclerotic plaques increased significantly after intraperitoneal compared with intravenous injection (*P*<0.01). In vivo MRI showed an increased uptake of NP-HDL into atherosclerotic lesions after intraperitoneal injection, which was confirmed by ex vivo MRI, x-ray fluorescence microscopy, confocal fluorescence microscopy, and histological analysis.

Conclusions—In vivo MRI and ex vivo multimodal imaging of atherosclerotic plaque using NP-HDL is feasible, and intraperitoneal application improves the uptake within vessel wall lesions compared with intravenous injection. (Circ Cardiovasc Imaging. 2014;7:303-311.)

Key Words: atherosclerosis ■ magnetic resonance imaging ■ quantum dots

A therosclerosis remains the main cause of morbidity and mortality in industrialized and developing nations. Growing evidence suggests that the decisive factor determining atherosclerotic plaque vulnerability is the plaque configuration rather than the degree of luminal narrowing. ²

Clinical Perspective on p 311

Molecular imaging may offer a new diagnostic tool to discriminate stable and vulnerable atherosclerotic plaques at an early stage of disease and to improve the detection of morphological and functional abnormalities within the vessel wall.^{3,4} The major hallmarks of early atherosclerotic lesion formation are endothelial dysfunction and accumulation of large amounts of lipoprotein-derived cholesterol esters in macrophages within

DOI: 10.1161/CIRCIMAGING.113.000607

Received April 25, 2013; accepted November 27, 2013.

The Data Supplement is available at http://circimaging.ahajournals.org/lookup/suppl/doi:10.1161/CIRCIMAGING.113.000607/-/DC1.

Correspondence to Caroline Jung, MD, University Hospital Hamburg-Eppendorf, Department of Radiology, Martinistrasse 52, 20246 Hamburg, Germany. E-mail cjung@uke.de

© 2013 American Heart Association, Inc.

From the Departments of Diagnostic and Interventional Radiology (C.J., M.G.K., G.A., H.I.), Biochemistry and Molecular Cell Biology (B.F., M.H., P.N., J.H.), and Anatomy and Experimental Morphology (M.H.), University Medical Center Hamburg Eppendorf, Hamburg, Germany; Institute of Physical Chemistry, University of Hamburg, Hamburg, Germany (S.C.S., H.W.); Department of Electron Microscopy and Micro Technology, Heinrich-Pette Institute, Hamburg, Germany (O.T.B., R.R.); Deutsches Elektronen-Synchrotron, A Research Centre of the Helmholtz Association, Hamburg, Germany (T.D., A.M.); Department of Chemistry, Massachusetts Institute of Technology, Cambridge, MA (O.T.B.); and CELLS-ALBA Synchrotron Light Source, Barcelona, Spain (TD).

the vessel wall.⁵ Because high-density lipoprotein (HDL) plays a key factor in the transportation of cholesterol and removes cholesterol from macrophages in atherosclerotic plaques,^{6,7} lipoprotein-based nanoparticles mimicking HDL are a promising tool to specifically target atherosclerosis.^{5,8} The characteristics of HDL, that is, its small size, role in reverse cholesterol transport, and inhibition of oxidation and inflammation, make it the best candidate among other lipoproteins.^{9,10} Various HDL particles such as radioactively labeled HDL,¹¹ reconstituted HDL,¹² synthetic HDL,¹³ and HDL nanoparticles¹³ have been reported and used for the imaging of vulnerable atherosclerotic plaques. Furthermore, HDL has been labeled with gold for CT,¹⁴ with quantum dots (QDs) for fluorescent microscopy,¹³ and with gadolinium or superparamagnetic iron oxide nanoparticles (SPIOs)¹³ for MRI.

As far as contrast agents are concerned, the detection of early atherosclerotic plaques in vivo by MRI using SPIO-labeled HDL is still a challenge. The MRI signal within plaques of preclinical mouse models is often difficult to depict clearly because of the small amount of accumulated HDL_{SPIO}, the small size of the mouse aorta, and the protracted peak of accumulation that starts ≈ 24 hours after intravenous injection. ^{13,15}

To improve imaging modalities, we reconstituted human HDL and replaced the hydrophobic core of HDL with either QDs or SPIOs. To the best of our knowledge, the embedding of nanoparticles into reconstituted human HDL has not been reported previously and has only been described using synthetic HDL. By comparing 2 different application approaches, that is, intravenous and intraperitoneal injection, the aims of this study were:

- to synthesize and establish HDL for nanoparticle transport:
- 2. to evaluate the biodistribution by different imaging techniques and by colabeling with ⁵⁹Fe;
- 3. to investigate whether intraperitoneal injection of NP-HDL increases the accumulation of NP-HDL within the atherosclerotic plaque compared with intravenous injection using various in vivo and ex vivo imaging techniques, including x-ray fluorescence microscopy (XRF); and
- to evaluate MR relaxometry for the quantitative determination of NP-HDL_{59Fe-SPIO} accumulation compared with ⁵⁹Fe radioactivity measurements.

Methods

Synthesis of Nanoparticles

The synthesis of CdSe/CdS/ZnS nanoparticles (QDs) with a core size of 5 to 6 nm was performed by the injection of $\rm H_2S$ gas 16 in a typical procedure as described previously. 17 QDs were kindly provided by Prof. A. Eychmüller from the Institute of Physical Chemistry and Electrochemistry, TU Dresden, Germany. SPIOs with a core size of 7 nm were synthesized as described previously. 18

HDL Nanoparticles

Human HDL was isolated from normal human plasma (approved by Ärztekammer Hamburg, Germany) by sequential density gradient ultracentrifugation, and lipid concentrations were determined using commercial lipid detection kits (Roche Diagnostics GmbH, Mannheim, Germany). Then, 5 mg of lipids was extracted using 1 mL of chloroform/methanol (8:5 v/v) by vigorous shaking. Apolipoproteins were pelleted by centrifugation at 18 000g for 10 minutes. Supernatants

were harvested and the solvent removed under an ambient flow of nitrogen. For embedding, 10 mg of the lipid extract was dissolved in chloroform and mixed with 0.4 mg iron oxide nanoparticles, or with 5 mmol CdSe/CdS/ZnS core-shell-shell nanoparticles, or with 5 mg oxide nanoparticles (200 KBq/10 mg lipid). The solvent was removed and the NP-HDLs were resuspended in 4 mL PBS at 65°C, and 0.5 mg deoxycholic acid was added. NP-HDLs were formed by sonication 3 times for 4 minutes in 4 mL PBS. Aggregates were removed by filtration, first using a 450-nm filter followed by a 220-nm filter (Merck Millipore, Darmstadt, Germany). The NP-HDLs were concentrated using Amicon Ultra-4 Centrifugal Filter Units (Merck Millipore). An overview of the NP-HDL composition (cores: QD/SPIO/59Fe-SPIO), imaging modalities, and detection methods are provided in Figure 1.

Characterization of NP-HDL

For lipoprotein profiling, plasma or isolated HDLs were separated by FPLC using S6-superose columns (GE Healthcare), and the lipid levels were analyzed in each fraction. In the case of QD-labeled NP-HDL, individual fractions were collected after separating the nanoparticles by gradient density centrifugation, and the cholesterol and triglyceride concentrations in each fraction were analyzed by enzymatic lipid determination. To verify the incorporation of QDs into the lipid core, the fluorescence in the fractions of HDLs was measured after UV excitation. The hydrodynamic diameter of the NP-HDLs was determined by dynamic light scattering (DLS; Malvern Zeta Sizer Nano-ZS; Malvern Instruments Limited, Malvern, Worcestershire, United Kingdom). The integrity and structure of the iron oxide particles and the QDs have been described and shown recently by electron microscopy.¹⁷

Animals

All B6.129P2-apoE^{tm1Unc/J} (C57BL/6J background) mice (ApoE^{-/-}) were purchased from Charles River Laboratories/Jackson Laboratories, Bar Harbor, ME, and were bred within the Animal Unit of the University Hospital Hamburg Eppendorf. To develop atherosclerotic plaques, 12-month-old (mean age, 12±2 months) ApoE^{-/-} mice were exposed to a Western-type diet (EF R/M TD88137; ssniff GmbH) for ≥30 weeks (mean, 40±10 weeks) before the imaging experiments were performed. ApoE^{-/-} mice for radioactive biodistribution analysis were 8 months old and did not receive a Western-type diet.

Determination of Blood Clearance and Biodistribution of NP-HDL by Radioactive Measurements

For the gamma activity measurements performed in Hamburg, a whole-body radioactivity counter (HAMCO)^{20} was used. The iron oxide core was prelabeled with ^{59}Fe (NP-HDL $_{59\text{Fe-SPIO}}$). 19 NP-HDL $_{59\text{Fe-SPIO}}$ (400 μL) was injected either intraperitoneally (n=6) or intravenously into the tail vein (n=6) of ApoE $^{-/-}$ mice. The total amount of applied radioactivity was measured immediately after injection. Blood samples were taken 1, 5, 20, 40, 60, 90, 120, 180, and 220 minutes after injection to determine blood clearance. For the biodistribution of NP-HDL $_{59\text{Fe-SPIO}}$, the mice were perfused with 4% paraformaldehyde 220 minutes postinjection, and activity measurements were performed on the aorta, spleen, kidney, lung, muscle, heart, liver, peritoneal macrophages, and femur.

MR Image Analysis

MR image analysis was performed using ImageJ (Image Processing and Analysis in Java, version 1.44p; National Institutes of Health, Bethesda, MD). To evaluate the signal enhancement index (SEI) of the aortic wall, liver, and spleen quantitatively, the percent decrease (%SEI $_{\rm rel}$) in relation to muscle tissue was calculated according to the equation, %SEI $_{\rm rel}$ =(SR $_{\rm post}/SR_{\rm pre}$ -1)×100, with SR=SI $_{\rm aortic\,wall}/SI_{\rm muscle}$, and was determined from the signal ratio (SR) of the signal intensities (SI).

NP-HDL	4900.00	And Market	
core	quantum dots (QD)	superparamagnetic iron oxides (SPIO)	59Fe-SPIO
lipids	Phospholipids	Triglycerides	Cholesterol
imaging modalitiy & detection methods	Optical imaging	MRI	MRI
	X-ray fluorescence microscopy	X-ray fluorescence microscopy	X-ray fluorescence microscopy
	Fluorescence microscopy	Light microscopy (Prussian Blue staining)	Light microscopy (Prussian Blue staining)
			γ -counter/ HAMCO

Jung et al

Figure 1. Schematic composition of imaging and detection methods for NP-HDL. Nanoparticles (QD, SPIOs, or 59Fe-SPIOs) were embedded into the lipid core of HDL by sonification. The different nanoparticle properties demand specific imaging modalities and detection methods for the confirmation of NP-HDL in tissues. HDL indicates high-density lipoprotein; NP-HDL, nanoparticle-labeled HDL; QD, quantum dots; and SPIO, superparamagnetic iron oxide nanoparticles.

These calculations were performed on the T2*-weighted MR image of the T2*-weighted MR relaxometry using the third echo (TE=2.97 ms). T2* MR relaxometry maps were generated using a custom-made software plugin for ImageJ. 21 Δ R2* was assessed by the following equation: Δ R2*=R2* $_{post}$ -R2* $_{post}$ -R2* $_{post}$ with R2*[s-1]=1/T2*[ms]×1000.

Statistical Analysis

Data are presented as mean±SD. For statistical analyses of pre and post images, a paired *t*-test was used. For all other statistical analyses, a 2-tailed unpaired Student *t*-test was performed. A value of *P*<0.05 was considered statistically significant.

Ethical Statement

All animal experiments were supervised by the institutional animal welfare officer and approved by the local licensing authority (Behörde für Soziales, Familie, Gesundheit und Verbraucherschutz; Amt für Gesundheit und Verbraucherschutz, Hamburg, Germany; project no. 33/10).

The methods used for cell incubation and competitive inhibition experiments, isolation of peritoneal macrophages, MRI, histological analysis, fluorescence microscopy, XRF, and transmission electron microscopy are described in the Data Supplement.

Results

Characterization of NP-HDL

As seen from the FPLC profile of human plasma and isolated HDLs, the concentration gradient of cholesterol and triglyceride of the isolated HDL fraction overlapped with the HDL gradient from human plasma (Figure 2A and 2B). No contamination with other lipoproteins such as low-density lipoprotein was detected.

After separating NP-HDL $_{\rm QD}$ by density gradient ultracentrifugation, individual fractions were collected and cholesterol was quantified. The cholesterol measurements of NP-HDLs corresponded to those from loaded HDLs. Next to some bigger aggregates, a cholesterol peak was detected in HDL fractions

(fraction ≈15; Figure 2C). The measured fluorescence after UV excitation in the HDL fraction indicates the successful incorporation of QDs into the recombinant HDL, whereas no fluorescent signal was obtained from HDL fractions prepared without QDs (Figure 2D).

DLS revealed that empty NP-HDL had similar size compared with native HDL (8–12 nm; Figure 2E). After incorporation of QDs or SPIOs into the lipid core, NP-HDL particles were slightly bigger in terms of the hydrodynamic diameter. Moreover, TEM analysis determined that if the lipid envelope stayed stable during TEM preparation, only 1 single nanocrystal was embedded into the lipidcore of NP-HDL_{SPIO} (Figure I in the Data Supplement).

Cell incubation experiments illustrated the uptake of NP-HDL $_{\rm QD}$ in murine macrophages in vitro (Figure II in the Data Supplement). The fluorescence signal of NP-HLD $_{\rm QD}$ decreased by competitive inhibition in the presence of a 20× higher concentration of unlabeled NP-HDL.

MRI In Vivo Biodistribution

In T2*-weighted MR images, the intravenously administered NP-HDL_{SPIOs} were detected in the liver and spleen and led to a reduced signal, resulting in a shortening of T2* relaxation time (P<0.001; Figure 3; see Table). A signal decrease in the liver and spleen was also observed after intraperitoneal injection of NP-HDL_{SPIO}, and a shortening of T2* relaxation time was noted (P<0.001). The calculated Δ R2* of the liver was significantly lower (P<0.05) when particles were injected intraperitoneally. No significant difference in Δ R2* was detected in the spleen.

MR measurements were confirmed by histology showing that the particles had lodged within the liver and the spleen after intravenous and intraperitoneal injection. To investigate the lower uptake of NP-HDL into the liver after intraperitoneal application, ⁵⁹Fe radioactive measurements were performed.

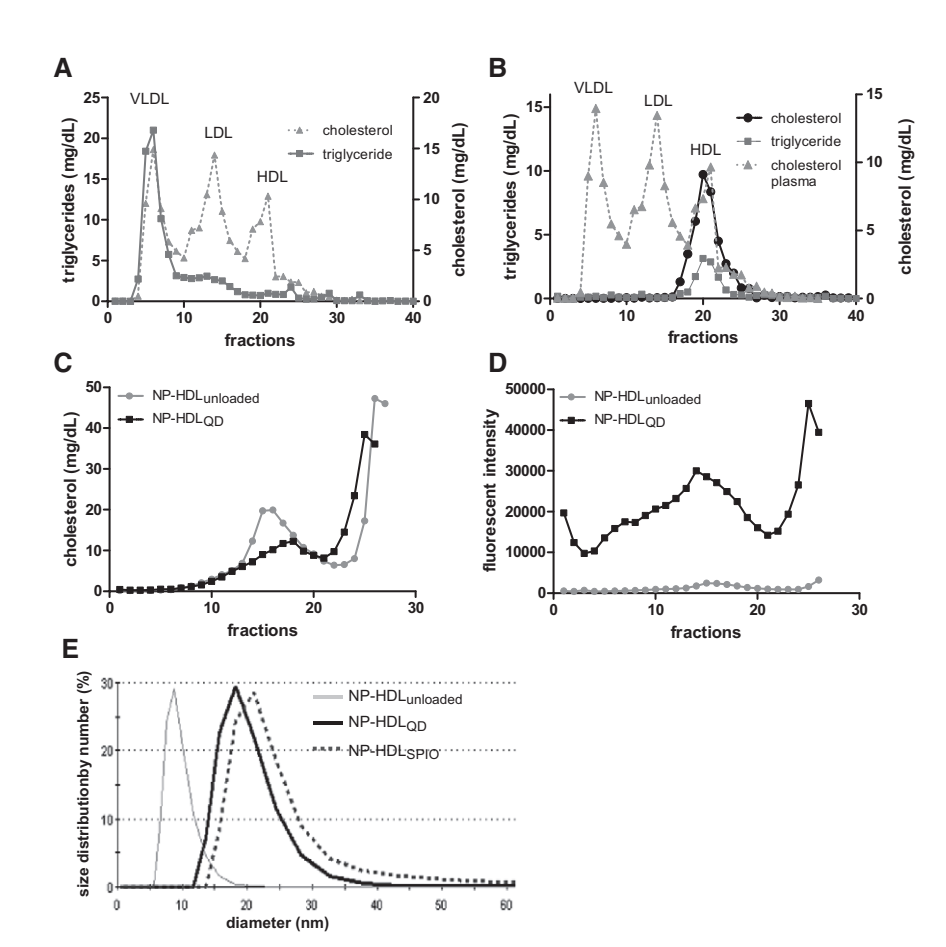


Figure 2. Characterization of human lipids, HDL, and NP-HDL. A, FPLC of the lipoprotein profile from human plasma. B, FPLC profile from isolated HDL: the concentration gradients of cholesterol and triglyceride of isolated HDL fractions overlap with the HDL gradient from human plasma. C, After separating the NP-HDL $_{\rm QD}$ by gradient density centrifugation, individual fractions were collected, and cholesterol was quantified. A cholesterol peak in HDL fractions (fractions ≈15) was detected; however, larger micelle aggregates containing HDL lipid components could also be detected. D, Fluorescence intensity after UV excitation in the fraction of HDL indicates the incorporation of QDs into prepared HDL. E, Dynamic light scattering of unloaded NP-HDL and native HDL demonstrated a similar size (8-12 nm), whereas embedding of QD or SPIO into the lipid core of NP-HDL increased the mean diameter up to 18 to 20 nm. HDL indicates high-density lipoprotein; NP-HDL, nanoparticle-labeled HDL; QD, quantum dots; and SPIO, superparamagnetic iron oxide nanoparticles.

Determination of Blood Clearance and Biodistribution by Radioactive Measurements

The activity in blood after intravenous injection of NP-HDL $_{59\mathrm{FeSPIO}}$ into the tail vein showed a biphasic profile over time (Figure 4A). In the first 30 minutes, rapid clearance occurred with <10% of the activity remaining in the blood by that time point, followed by delayed clearance during the second and third hour.

When NP-HDL_{59FeSPIOs} were injected intraperitoneally, the activity in blood increased far more slowly, reaching the same level when applied intravenously, but not until 40 minutes postinjection. The second part of the curve declined in parallel to the intravenous injection activity curve, resulting in similar blood clearance.

The final biodistribution pattern of NP-HDL_{59FeSPIO} after intravenous and intraperitoneal application in mice looked similar (Figure 4B). The highest activity uptake was measured in the liver and spleen, followed by the femur, aorta, and in the peritoneal macrophages in the case of intraperitoneal injection. However, some differences were detected depending on the mode of application in the liver, where the uptake was significantly higher after intravenous application (P<0.001), and in the aorta with a significant higher uptake of NP-HDL_{59FeSPIO} after intraperitoneal application (P<0.01; Figure 4C). The increased accumulation within the spleen after intraperitoneal injection was not significant.

Fluorescence Microscopy

Figure 5 shows the biodistribution of NP-HDL_{QD} after intravenous and intraperitoneal application using ex vivo fluorescence

microscopy. Twenty-four hours post–intravenous or intraperitoneal injection, confocal microscopy revealed that when NP-HDL $_{\rm QD}$ was applied intraperitoneally, the fluorescent signal increased in peritoneal macrophages (Figure 5E, indicated in red) compared with the intravenous delivery of NP-HDL $_{\rm QD}$ (Figure 5A). Nevertheless, after both application approaches, NP-HDL $_{\rm QD}$ was found in the spleen (Figure 5B and 5F), in the liver (Figure 5C and 5G), and in atherosclerotic lesions. In Figure 5D and 5H, the view into the abdominal aorta is shown with the atherosclerotic plaque bulging out into the lumen. No red fluorescence was detectable in the spleen, liver, and atherosclerotic plaque when saline was injected (Figure III in the Data Supplement).

MR Plaque Imaging

Figure 6 shows an example of in vivo MR plaque imaging, in which the uptake of NP-HDL $_{\rm SPIO}$ into an atherosclerotic lesion is demonstrated after intraperitoneal application. Because of the T2/T2* properties of NP-HDL $_{\rm SPIO}$, a signal drop occurred in the aortic wall with a mean signal drop of $10\pm11.7\%$ (Figure 6A and 6E). However, the measured SR $_{\rm pre}$ and SR $_{\rm post}$ were not significantly different. Atherosclerotic lesions after intravenous application could not be detected by MRI (data not shown).

To verify the uptake of NP-HDL_{SPIO} into the vessel wall after intraperitoneal injection, aortas were removed and imaged ex vivo by MRI. The T2-weighted images showed a clear decrease in signal intensity in the aortic wall of the aorta post-NP-HDL $_{\rm SPIO}$ in comparison to the uninjected aorta

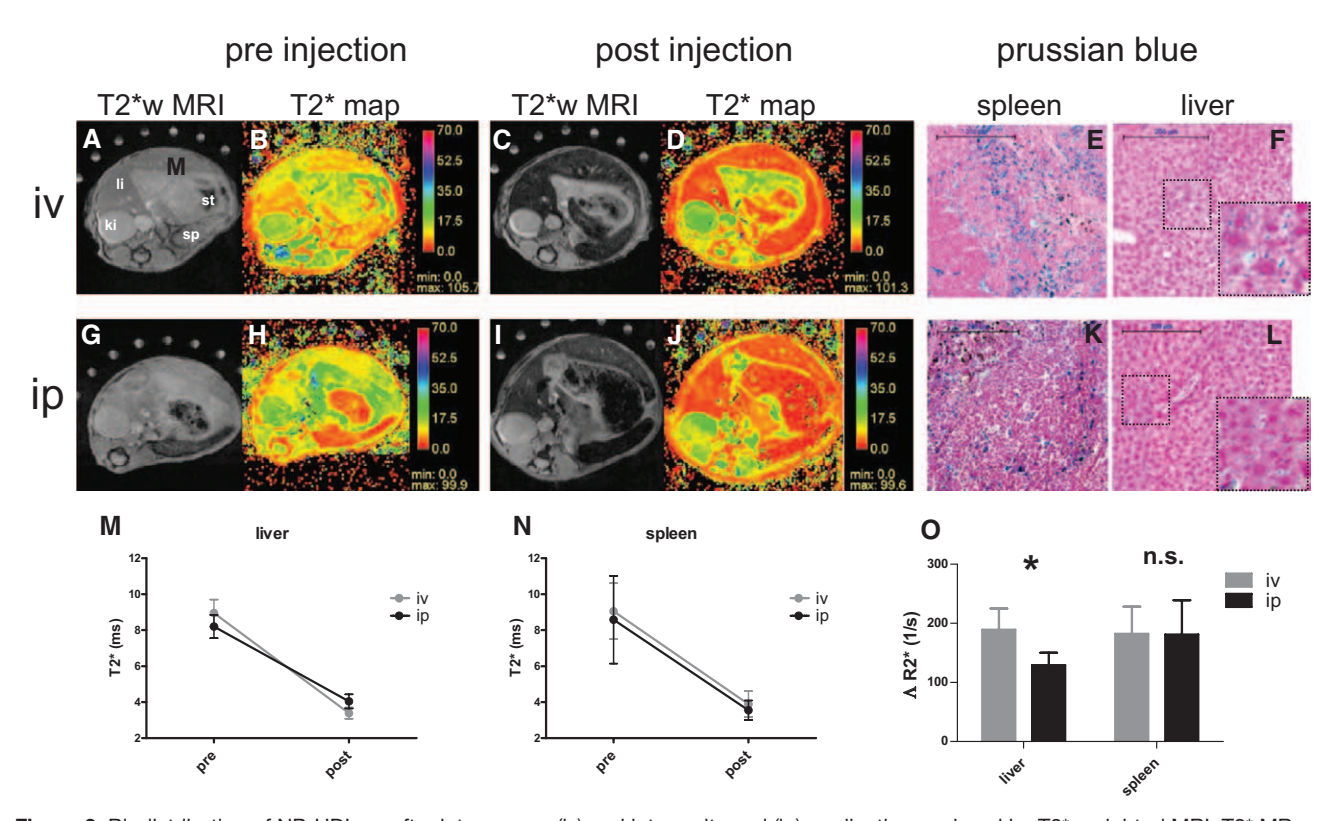


Figure 3. Biodistribution of NP-HDL_{SPIO} after intravenous (iv) and intraperitoneal (ip) application analyzed by T2*-weighted MRI, T2* MR relaxometry, and Prussian blue staining. **A** to **F**, T2*-weighted MRI and corresponding T2* relaxometry map before (**A** and **B**) and 24 h after (**C** and **D**) the iv application of NP-HDL_{SPIO} showed a strong signal decrease in liver and spleen, as confirmed with histological sections of the spleen (**E**) and liver (**F**) after Prussian blue staining, where the intracellular iron oxide aggregates of NP-HDL_{SPIO} appear blue (ki indicates kidney; li, liver; sp, spleen; and st, stomach). **G** to **L**, After ip application of NP-HDL_{SPIO}, a similar effect could be observed by T2*weighted MRI and T2* relaxometry map before (**G** and **H**) and 24 h after (**I** and **J**) inoculation with a decrease in signal intensity in the spleen and liver. Corresponding histological sections after Prussian blue staining revealed a similar intracellular accumulation of NP-HDL_{SPIO} in spleen (**K**) and liver (**L**). **M** and **N**, T2* relaxation times of the liver tissue showed a stronger decrease after iv (pre: 8.7±0.9 ms; post: 3.3±0.3 ms) than after ip injection (pre: 7.9±0.6 ms; post: 4.1±0.4 ms), whereas the reduction in T2* values in the spleen was comparable for both application approaches (iv—pre: 9.1±0.4 ms; post: 3.6±0.6 ms; ip—pre: 8.5±3.2 ms; post: 3.3±0.5 ms). **O**, Resulting ΔR2* of the liver was significantly higher for iv than ip injection (P<0.05), whereas $\Delta R2$ * of the spleen showed no significant differences (mean±SD; *P<0.05; n.s. indicates not significant). NP-HDL indicates nanoparticle-labeled high-density lipoprotein; and SPIO, superparamagnetic iron oxide nanoparticles.

(Figure 6B and 6F). The T2* relaxation map showed a significantly (P<0.01) shorter T2* relaxation time post–intraperitoneally injected aorta (6.9±1.19 ms) than the uninjected aorta (9.4±0.95 ms; Figure 6C and 6G).

Prussian blue staining confirmed the successful uptake of $NP-HDL_{SPIO}$ into atherosclerotic lesions. Although iron

Table. MRI Analyses

	SEI _{rel} , %	T2*, ms	Δ R2*, mmol/s
Intravenous			
Liver	72.2±9.9	Pre 8.7±0.9	189±36.3
		Post 3.3±0.3	
Spleen	77.3±6.9	Pre 9.1±0.4	182±46.3
		Post 3.6±0.6	
Intraperitoneal			
Liver	56.9±2.7	Pre 7.9±0.6	129±21.1
		Post 4.1±0.4	
Spleen	64.8±11.9	Pre 8.5±3.2	181±58.1
		Post 3.3±0.5	

SEI indicates signal enhancement index.

in SPIO appeared as a blue stain within the aortic plaque (Figure 6H), the control (saline only) showed no staining (Figure 6D).

X-Ray Fluorescence Microscopy

When XRF was performed, selenium was clearly detected within the atherosclerotic lesion after injection of NP-HDL $_{\rm QD}$ (Figure 7A), whereas no selenium signal was generated when NP-HDL $_{\rm SPIO}$ was applied. The background signal of zinc and sulfur naturally distributed in the tissue was too strong to separate from the signal enhancement created by NP-HDL $_{\rm QD}$ (Figure 7). Similar to zinc and sulfur, the basic iron background in tissue was too high to visualize and clearly distinguish by XRF the accumulation of iron resulting from NP-HDL $_{\rm SPIO}$ injection (Figure 7B).

Discussion

In this study, we established the preparation of recombinant NP-HDL based on human lipoproteins, which were similar to native HDLs with regard to lipid composition and size. Organ biodistribution and blood clearance of the nanoparticles

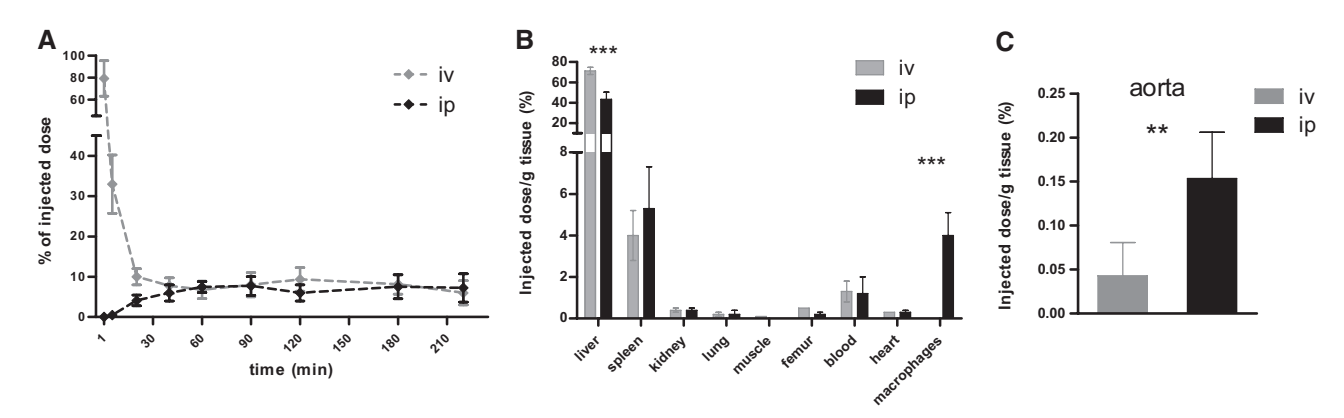


Figure 4. In vivo blood clearance and biodistribution of NP-HDL_{SSFeSPIO}. **A**, After intravenous (iv) injection, blood concentration showed a biphasic decrease with an accelerated clearance in the first 30 min, followed by a slowdown up to 60 min. In contrast, intraperitoneal (ip) injection showed a slow increase up to 1 h. Both application approaches resulted in a nearly steady-state concentration of NP-HDL_{SSFeSPIO} for ≥3 h. **B**, The highest uptake of NP-HDL_{SSFeSPIO} could be measured in the liver, followed by the spleen. Statistically significant differences (***) in the uptake between iv and ip application were detectable in liver, peritoneal macrophages, and aorta. **C**, After cleaning the aorta from surrounding connective tissue, the uptake of NP-HDL_{SSFeSPIO} was significant higher after ip than iv injection (**). (mean±SD; **P<0.01; ***P<0.001). NP-HDL indicates nanoparticle-labeled high-density lipoprotein; and SPIO, superparamagnetic iron oxide nanoparticles.

after intravenous and intraperitoneal injections were analyzed using ⁵⁹Fe-labeled NP-HDL_{SPIO}. A significantly higher uptake of NP-HDL_{SPIO} into the atherosclerotic lesions in ApoE^{-/-} mice was achieved after intraperitoneal injection. The uptake of NP-HDL_{QD} and NP-HDL_{SPIO} into the organs after intraperitoneal application was visualized by fluorescence microscopy and MRI. Although in vivo MRI of NP-HDL_{SPIO} within atherosclerotic lesions is still challenging, ex vivo MRI, XRF, confocal fluorescence microscopy (CFM), and Prussian blue staining of aortic specimens clearly indicated the uptake of NP-HDL into the atherosclerotic lesions. Therefore, the visualization of plaques using NP-HDLs by different imaging modalities is feasible.

The physical properties of recombinant NP-HDLs are very similar to those of endogenous HDL. The detection of fluorescence in the same fraction as native HDL indicates the correct incorporation of QDs into the prepared NP-HDL. Nevertheless, some material was also detected in the fractions containing larger-sized particles. Similar results have also been described by Frias et al²² and can be explained by the fusion of HDL micelles. Because of the preparation process, it is possible to embed >1 nanoparticle into the hydrophobic core of HDL. This can lead to bigger micelles containing HDL lipid components. To separate these bigger HDL micelles from NP-HDL, filtration was performed before NP-HDLs were used in experiments. DLS analysis revealed that loaded

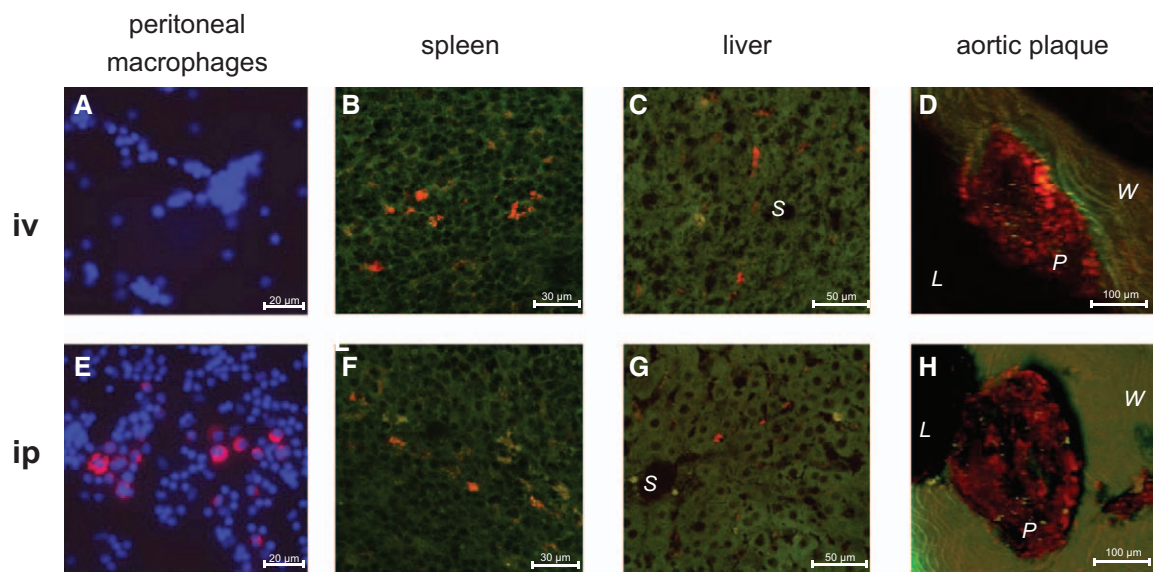


Figure 5. Biodistribution of NP-HDL $_{QD}$ after intravenous and intraperitoneal application using ex vivo fluorescence microscopy. A to **D**, 24 h after intravenous application, no accumulation of NP-HDL $_{QD}$ could be detected in peritoneal macrophages (**A**), whereas the particles accumulated in spleen (**B**), liver (**C**), and atherosclerotic plaques (**D**). **E** to **H**, 24 h after intraperitoneal application, NP-HDL $_{QD}$ was taken up by peritoneal macrophages (**E**). Comparable to intravenous injection, NP-HDL $_{QD}$ accumulated in spleen (**F**), liver (**G**), and atherosclerotic plaques (**H**). Red fluorescence signal represents NP-HDL $_{QD}$, green signal the autofluorescence of the tissue; peritoneal macrophages are stained with DAPI (blue). L indicates aortic lumen; P, atherosclerotic plaque; S, liver sinosuid; and W, aortic wall. NP-HDL indicates nanoparticle-labeled high-density lipoprotein; and QD, quantum dots.

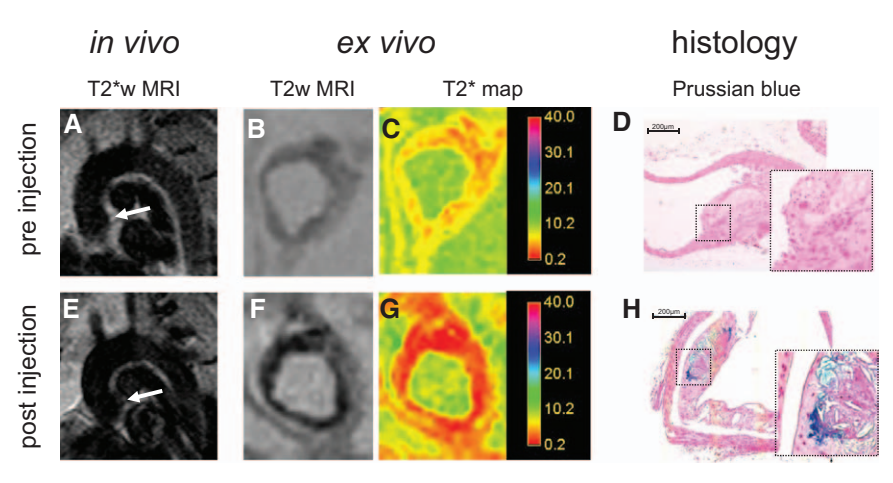


Figure 6. MRI and MR relaxometry of atherosclerotic plagues in vivo and ex vivo in comparison to histology. T2*-weighted MRI of the aortic arch of ApoE-/- mice before (A) and 24 h post-intraperitoneal injection (\mathbf{E}) of NP-HDL $_{\mathrm{SPIO}}$. Arrows indicate signal decrease within the aortic wall because of the uptake of NP-HDL_{SPIO}. Ex vivo T2*-weighted transverse MRI of the aorta before (B) and after (F) NP-HDL_{SPIO} application and corresponding T2* relaxation time maps (C and G). After $NP-HDL_{SPIO}$ injection, the aorta showed a stronger signal decrease with shortened T2* values (G). Prussian blue stains of aortic sections of mice injected with NP-HDL_{SPIO} revealed the presence of particles within the atherosclerotic plaques of the aortic vessel wall (H), whereas no

iron appears in the aortic wall of uninjected mice (**D**). NP-HDL indicates nanoparticle-labeled high-density lipoprotein; and SPIO, superparamagnetic iron oxide nanoparticles.

NP-HDL was slightly larger than unloaded HDL because of the core size of incorporated nanoparticles (QD, 5–6 nm; SPIO, 7 nm). Nevertheless, the lipid configuration and the surface of NP-HDLs were similar to endogenous HDL, and the slightly larger size should not be detrimental to plaque penetration, because even larger nanoparticle contrast agents (eg, 38-nm magnetic nanoparticles)²³ and larger biomolecules such as low-density lipoproteins (≈20 nm) can penetrate the endothelial barrier.

The rapid plasma clearance of NP-HDL after intravenous application in the first 30 minutes is in accordance with previous studies. 11 Nevertheless, ≈5% of the injected dose of radioactivity was still present in the plasma 3 hours after injection, which may be because of free radioactive iron as well as redistribution between different organs. Although the initial biodistribution data after intravenous and intraperitoneal application look similar in our experiments, we observed a significantly higher uptake of NP-HDL within the liver (P<0.001) after intravenous injection. The higher uptake of intravenously injected NP-HDL into the liver led to a more rapid degradation of NP-HDL in the liver. It has been shown by previous studies¹⁹ that when radioactive-labeled SPIOs prepared in the same way as the present study were embedded into triglyceride-rich lipoproteins, lipoproteins underwent faster degradation in the liver. We assume that the radioactivity we observed in the blood 40 minutes after intravenous application was because of free circulating iron. After intraperitoneal injection, blood levels initially rose as NP-HDL found their way into the blood, and we observed a slower uptake of NP-HDL into the bloodstream, such that NP-HDLs were not dismantled as quickly by the liver, and most of the particles remained embedded in the lipid core of HDL 40 minutes after injection. This resulted in a significantly higher uptake of NP-HDL in the atherosclerotic lesions (P<0.01) after intraperitoneal administration. Similar pharmacokinetics of intraperitoneal and intravenous administration were observed by Allen et al²⁴ and van Zanten-Przybysz et al.²⁵ However, Allen et al used liposomes 100 to 150 nm in size for the therapeutic application of liposomal drug delivery systems, whereas van Zanten-Przybysz analyzed the route of administration of a monoclonal antibody (MOv 18) to target ovarian cancer. Allen et al reported that intraperitoneal injection of liposomes resulted in almost constant blood liposome levels for a period of several hours, which makes desirable the use of liposomes as a sustained-release system in vivo.²⁶

Using T2* relaxometries for biodistribution analysis by MRI enabled us not only to visualize but also to quantify the accumulation of NP-HDL_{SPIO} in the liver and spleen. MRI results confirmed the lower uptake of NP-HDL_{SPIO} in the liver by the significantly lower Δ R2* relaxation rate (P<0.01) after intraperitoneal application.

The uptake of NP-HDL into the atherosclerotic lesions was demonstrated by different imaging techniques, that is, ex vivo MRI, XRF, CFM, and light microscopy of Prussian

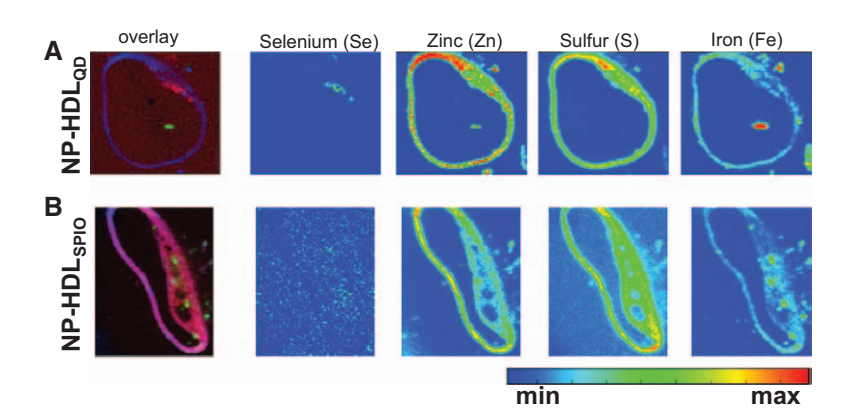


Figure 7. X-ray fluorescence maps of 20-μm cross-sections of mice aorta after 24 h in vivo treatment with NP-HDL $_{\!\scriptscriptstyle \rm QD}$ (A) and NP-HDL $_{\!\scriptscriptstyle \rm SPIO}$ (B) recorded at photon energy of 13.4 keV. The first column shows the distribution of 3 analyzed elements within the aortic wall in overlay mode: selenium (red), zinc (blue), and iron (green) in A and sulfur (red), zinc (blue), and iron (green) in B. Selenium as part of the hydrophobe CdSe/CdS/ZnS coreshell-shell nanoparticle of QD was detectable with increased concentrations within the plaque only after NP-HDL $_{\!\scriptscriptstyle QD}$ injection, whereas Zn, S, and Fe as natural elements of the aortic wall were not clearly distinguishable from the applied particles. Image sizes: 900×840 μm (A), 1120×1080 μm (B). Pixel size corresponds to 10×10 µm, and dwell time 1 s per pixel. Color bar represents the number of counts.

blue-stained aorta specimens. Despite respiratory and pulse oximetry gating to minimize motion artefacts for in vivo MRI analysis to obtain improved image quality, the noninvasive detection of NP-HDL_{SPIO} by in vivo MRI remains challenging. Previous studies have attempted to visualize the in vivo uptake of SPIO-labeled HDL into plaques by MRI.¹³ However, these studies did not use ex vivo MRI to confirm the data and did not quantify the signal drop by estimating the T2* time. Signal differences in our study for vessel wall lesions in pre- and post-MR in vivo images were not significant. Motion and susceptibility artefacts caused by breathing, vessel pulsation, and gut movement made R2 and R2* quantification in vivo very difficult, in particular for small regions of interest such as atherosclerotic plaques in ApoE^{-/-} mice.²⁷ By using ex vivo MRI, movement artefacts can be avoided and the results obtained in vivo can be easily validated. Moreover, ex vivo MRI allows for a longer scan time to achieve a higher signal-to-noise ratio and a greater resolution, resulting in better detection of plaques and better quantification of NP-HDL_{SPIO} uptake within the plaque.

XRF analysis provided a precise elemental distribution of aorta tissues in high spatial resolution and could be obtained solely by synchrotron techniques. It is feasible to achieve an elemental map distribution in sub-ppm concentrations. This approach shows the colocalization of selenium, exclusively present in NP-HDL $_{\rm QD}$ and, when incorporated, in atherosclerotic plaques (Figure 7A). Moreover, the XRF approach confirmed the results obtained by MRI, CFM, and Prussian blue staining.

Several limitations influenced the outcome of the present study. To generate severe atherosclerotic lesions in living animals, ApoE^{-/-} mice were used at an old age and had to be fed a Western-type diet. It is known that a long-term Western diet use will lead to the calcification of plaques.²⁸ Calcium carbonate exhibits a short T2 and T2* time by itself. If the plaques were already calcified at the time of NP-HDL_{SPIO} injection, the T2 and T2* time would be too short to observe an effect because of SPIOs in NP-HDL_{SPIO}. Although resembling an important aspect of human pathology, this effect could interfere with T2* measurements. Moreover, as the number of animals for MR analysis was relatively small, resulting in high standard deviations, the detection of atherosclerotic lesions after NP-HDL_{SPIO} application by MRI should be presently seen only as a proof of concept.

To summarize, we have successfully prepared NP-HDLs for the detection of atherosclerotic plaques under multimodal imaging. We have shown that NP-HDLs have similar characteristics as endogenous HDL. Nanoparticles (QD and SPIO) were incorporated successfully into the hydrophobic core, and the labeled NP-HDL had desired lipid composition such that it mimicked the native HDL. Using NP-HDL $_{59FeSPIO}$, we were able to investigate blood clearance and biodistribution of injected NP-HDL, and even more importantly, we quantified the accumulation of radiolabeled nanoparticles within the atherosclerotic plaques. In addition, we confirmed the uptake of NP-HDL using MRI, XRF, CFM, and light microscopy. Moreover, the estimation of T2* and Δ R2* allowed the quantification of signal drop due to the accumulation of NP-HDL $_{SPIO}$. This is also the first

report showing the detection of elements of NP-HDL in atherosclerotic lesions by XRF.

Acknowledgments

We wish to thank D. Wendt, S. Ehret, A. Japke, J. Kemmling, and H. Hermann for excellent technical assistance. We would like to thank Dr K. Appel for assistance in using the beamline, and B. Mollwitz and K. Brueggemann for assistance in preparing NP-HDL.

Sources of Funding

This work was supported by the Hamburg State Excellence Initiative's Nanotechnology in Medicine (NAME), by the Bundesministerium für Forschung und Technologie (BMBF, TOMCAT, project number 01 EZ 0824), by grants from the Deutsche Forschungsgemeinschaft to P.N., J.H., and H.W. (SPP1313). J.H. is supported by EU FP7 project RESOLVE (FP7-HEALTH-2012–305707). T.D. performed x-ray fluorescence experiments at the DORIS III light source (beamline L), a member of the Helmholtz Association, supported through a long-term project II-20080239. O.T.B. is supported by an EMBO long-term fellowship. The funding sources played no role in the study design, data collection, data management, data analysis, data interpretation, article preparation, article review, or article approval.

Disclosures

None.

References

- Naghavi M, Libby P, Falk E, Casscells SW, Litovsky S, Rumberger J, Badimon JJ, Stefanadis C, Moreno P, Pasterkamp G, Fayad Z, Stone PH, Waxman S, Raggi P, Madjid M, Zarrabi A, Burke A, Yuan C, Fitzgerald PJ, Siscovick DS, de Korte CL, Aikawa M, Airaksinen KE, Assmann G, Becker CR, Chesebro JH, Farb A, Galis ZS, Jackson C, Jang IK, Koenig W, Lodder RA, March K, Demirovic J, Navab M, Priori SG, Rekhter MD, Bahr R, Grundy SM, Mehran R, Colombo A, Boerwinkle E, Ballantyne C, Insull W Jr, Schwartz RS, Vogel R, Serruys PW, Hansson GK, Faxon DP, Kaul S, Drexler H, Greenland P, Muller JE, Virmani R, Ridker PM, Zipes DP, Shah PK, Willerson JT. From vulnerable plaque to vulnerable patient: a call for new definitions and risk assessment strategies: part II. Circulation. 2003;108:1772–1778.
- Fuster V, Badimon L, Badimon JJ, Chesebro JH. The pathogenesis of coronary artery disease and the acute coronary syndromes (1). N Engl J Med. 1992;326:242–250.
- Sirol M, Itskovich VV, Mani V, Aguinaldo JG, Fallon JT, Misselwitz B, Weinmann HJ, Fuster V, Toussaint JF, Fayad ZA. Lipid-rich atherosclerotic plaques detected by gadofluorine-enhanced in vivo magnetic resonance imaging. Circulation. 2004;109:2890–2896.
- Honda M, Kawahara I, Kitagawa N, Tsutsumi K, Morikawa M, Hayashi T, Nagata I. Asymptomatic carotid artery plaques: use of magnetic resonance imaging to characterize vulnerable plaques in 6 cases. Surg Neurol. 2007;67:35–39.
- Heeren J, Bruns O. Nanocrystals, a new tool to study lipoprotein metabolism and atherosclerosis. Curr Pharm Biotechnol. 2012;13:365–372.
- 6. Lusis AJ. Atherosclerosis. Nature. 2000;407:233-241.
- Linsel-Nitschke P, Tall AR. HDL as a target in the treatment of atherosclerotic cardiovascular disease. Nat Rev Drug Discov. 2005;4:193–205.
- Lobatto ME, Fuster V, Fayad ZA, Mulder WJ. Perspectives and opportunities for nanomedicine in the management of atherosclerosis. *Nat Rev Drug Discov*. 2011;10:835–852.
- Feig JE, Shamir R, Fisher EA. Atheroprotective effects of HDL: beyond reverse cholesterol transport. Curr Drug Targets. 2008;9:196–203.
- Florentin M, Liberopoulos EN, Wierzbicki AS, Mikhailidis DP. Multiple actions of high-density lipoprotein. Curr Opin Cardiol. 2008;23:370–378.
- Shaish A, Keren G, Chouraqui P, Levkovitz H, Harats D. Imaging of aortic atherosclerotic lesions by (125)I-LDL, (125)I-oxidized-LDL, (125)I-HDL and (125)I-BSA. *Pathobiology*. 2001;69:225–229.
- Frias JC, Williams KJ, Fisher EA, Fayad ZA. Recombinant HDL-like nanoparticles: a specific contrast agent for MRI of atherosclerotic plaques. *J Am Chem Soc.* 2004;126:16316–16317.
- Cormode DP, Skajaa T, van Schooneveld MM, Koole R, Jarzyna P, Lobatto ME, Calcagno C, Barazza A, Gordon RE, Zanzonico P, Fisher

- EA, Fayad ZA, Mulder WJ. Nanocrystal core high-density lipoproteins: a multimodality contrast agent platform. *Nano Lett.* 2008;8:3715–3723.
- Cormode DP, Roessl E, Thran A, Skajaa T, Gordon RE, Schlomka JP, Fuster V, Fisher EA, Mulder WJ, Proksa R, Fayad ZA. Atherosclerotic plaque composition: analysis with multicolor CT and targeted gold nanoparticles. *Radiology*. 2010;256:774–782.
- Ruehm SG, Corot C, Vogt P, Kolb S, Debatin JF. Magnetic resonance imaging of atherosclerotic plaque with ultrasmall superparamagnetic particles of iron oxide in hyperlipidemic rabbits. *Circulation*. 2001;103:415–422.
- Talapin DV, Shevchenko EV, Murray CB, Kornowski A, Förster S, Weller H. CdSe and CdSe/CdS nanorod solids. J Am Chem Soc. 2004;126:12984–12988.
- Bruns OT, Ittrich H, Peldschus K, Kaul MG, Tromsdorf UI, Lauterwasser J, Nikolic MS, Mollwitz B, Merkel M, Bigall NC, Sapra S, Reimer R, Hohenberg H, Weller H, Eychmüller A, Adam G, Beisiegel U, Heeren J. Real-time magnetic resonance imaging and quantification of lipoprotein metabolism in vivo using nanocrystals. Nat Nanotechnol. 2009;4: 193–201
- Hyeon T, Lee SS, Park J, Chung Y, Na HB. Synthesis of highly crystalline and monodisperse maghemite nanocrystallites without a size-selection process. J Am Chem Soc. 2001;123:12798–12801.
- Freund B, Tromsdorf UI, Bruns OT, Heine M, Giemsa A, Bartelt A, Salmen SC, Raabe N, Heeren J, Ittrich H, Reimer R, Hohenberg H, Schumacher U, Weller H, Nielsen P. A simple and widely applicable method to 59Fe-radiolabel monodisperse superparamagnetic iron oxide nanoparticles for *in vivo* quantification studies. ACS Nano. 2012;6:7318–7325.
- Braunsfurth JS, Gabbe EE, Heinrich HC. Performance parameters of the Hamburg 4 pi whole body radioactivity detector. *Phys Med Biol*. 1977;22:1–17.

- Kaul MG, Ernst T, Adam G. qMaplt, an ImageJ-plugin, for quantitative multi-parametric analysis of DICOM images. *Proceedings of the ImageJ User and Developer Conference*. Mondorf-les-Bains, Luxembourg. 2012: 130
- Frias JC, Ma Y, Williams KJ, Fayad ZA, Fisher EA. Properties of a versatile nanoparticle platform contrast agent to image and characterize atherosclerotic plaques by magnetic resonance imaging. *Nano Lett.* 2006;6:2220–2224.
- Nahrendorf M, Jaffer FA, Kelly KA, Sosnovik DE, Aikawa E, Libby P, Weissleder R. Noninvasive vascular cell adhesion molecule-1 imaging identifies inflammatory activation of cells in atherosclerosis. *Circulation*. 2006;114:1504–1511.
- Allen TM, Hansen CB, Guo LS. Subcutaneous administration of liposomes: a comparison with the intravenous and intraperitoneal routes of injection. *Biochim Biophys Acta*. 1993;1150:9–16.
- van Zanten-Przybysz I, Molthoff CF, Roos JC, Verheijen RH, van Hof A, Buist MR, Prinssen HM, den Hollander W, Kenemans P. Influence of the route of administration on targeting of ovarian cancer with the chimeric monoclonal antibody MOv18: i.v. vs. i.p. *Int J Cancer*. 2001;92:106–114.
- Allen TM, Hansen C, Martin F, Redemann C, Yau-Young A. Liposomes containing synthetic lipid derivatives of poly(ethylene glycol) show prolonged circulation half-lives in vivo. *Biochim Biophys Acta*. 1991;1066:29–36.
- Kuhlpeter R, Dahnke H, Matuszewski L, Persigehl T, von Wallbrunn A, Allkemper T, Heindel WL, Schaeffter T, Bremer C. R2 and R2* mapping for sensing cell-bound superparamagnetic nanoparticles: in vitro and murine in vivo testing. Radiology. 2007;245:449–457.
- Reddick RL, Zhang SH, Maeda N. Atherosclerosis in mice lacking apo E. Evaluation of lesional development and progression. *Arterioscler Thromb*. 1994;14:141–147.

CLINICAL PERSPECTIVE

Atherosclerosis is the primary cause of heart disease and stroke, and it accounts for 50% of all deaths in Western societies. Furthermore, despite pharmacological intervention and lifestyle changes, cardiovascular disease continues to be the principal cause of death in the United States, Europe, and much of Asia. Given these severe health threats of atherosclerosis, noninvasive detection and characterization of plaques may be useful to detect patients at risk, or to monitor the efficacies of therapies. Growing evidence suggests that the decisive factor determining atherosclerotic plaque vulnerability is more dependent on the plaque configuration than on the degree of luminal narrowing. For this, it is necessary to develop new imaging strategies. Especially molecular imaging has the potential to identify vulnerable and high-risk plaques by diagnosing early atherosclerotic lesions and by accurately determining plaque composition. In this study, we used high-density lipoprotein (HDL) as contrast agent. Nanoparticle-labeled HDL takes the advantage of HDL's physiological role in participating in cholesterol efflux from tissues, including atheromatous plaques in vessels, and migrating in and out of atherosclerosis to provide contrast enhancement on MRI. By intraperitoneal injection, a higher accumulation in atherosclerotic vessel wall lesions could be observed.